A novel storage system for cooling stand-alone photovoltaic installations

I. Lillo-Bravo[a], M. A. Bobadilla[b], S. Moreno-Tejera[a], M. Silva-Pérez[a],

[a] *Department of Energy Engineering, University of Seville, Spain*

[b] *Andalusian Association for Research and Industrial Cooperation (AICIA), Spain*

Corresponding author

Address: Department of Energy Engineering, Escuela Técnica Superior de Ingeniería, University of Seville, Camino de los Descubrimientos s/n. 41092, Seville, Spain.

E-mail: isidorolillo@us.es

ABSTRACT

Stand-alone photovoltaic systems usually use batteries to adjust energy yield to energy demand. An alternative energy storage system for stand-alone photovoltaic installations is proposed for three cooling applications: air conditioning, food preservation and freezing. A thermally insulated storage tank with ammonia in saturated mixture phase is integrated into the vapour-compression cooling cycle. A thermodynamic model and an economic assessment based on typical costs and costs sensitivity are included to assess the proposed system performance in comparison with a conventional stand-alone photovoltaic system with a vapour-compression cycle. Results show the proposed storage strategy is an affordable option especially in hot climates and for food preservation and freezing applications.

Keywords: Solar energy, energy storage system, photovoltaic, solar cooling. ~~ammonia~~.

Nomenclature

A_{pv1} Required photovoltaic array area of the installation 1 per cooling unit (m^2/kWhc).

A_{pv2} Required photovoltaic array surface of the installation 2 per cooling unit (m^2/kWhc).

C_{t1} Installation 1 total costs (including tank and refrigerant costs but excluding the cooling cycle costs) per cooling unit (€/ kWh_c).

C_{t2} Installation 2 total costs (excluding the cooling cycle costs) per cooling unit (€/ kWh_c).

DoD Battery Depth of Discharge.

E_b Energy capacity of battery B in 10 discharging hours per cooling unit (Wh/kWhc).

E_{Baux} Energy capacity of auxiliary battery B_1 per cooling unit (Wh/kWhc).

E_{c1} Compressor energy consumption of the installation 1 per unit of kWh_c (kWh).

E_{c2} Compressor energy consumption of the installation 2 per unit of kWh_c (kWh).

EER1 Installation 1 Efficient Energy Ratio.

EER2 Installation 2 Efficient Energy Ratio.

E_{pv1} Energy required to the solar array of the installation 1 per unit of kWh_c (kWh).

E_{pv2} Energy required to the solar array of the installation 2 per unit of kWh_c (kWh).

g Acceleration due to the gravity (m/s^2).

H_p Drop pressure in the refrigerant circuit between point 9 and 10 of installation 1 (mwc).

h_i Specific enthalpy at the point i (kJ/kg).

m_{ref} Required refrigerant mass, per cooling unit (kg/kWhc).

P Auxiliary pump power (W).

P_b Battery cost per storage kWh (€/kWh).

P_{sa} PV array cost per m^2 (€/m^2)

P_{ref} Ammonia cost per kg (€/kg).

p_T Pressure to be withstood by the tank (Pa).

$p^{f+g}(T_e)$ Ammonia vapour pressure at evaporator temperature, T_e (Pa).

P_t Ammonia tank cost per unit of volume (€/m^3).

Q_L Cooling produced by the evaporator (kWh_c)

q_{V9} Volume flow rate of ammonia at point 9 of installation 1($\frac{m3}{s}$).

r Annual discount rate, %.

T_e Evaporator temperature (K).

V_T Volume of the refrigerant tank, per cooling unit (m^3/kWhc).

ρ_9 Ammonia density at point 9 of installation 1 (kg/m^3).

η_{cb} Mean battery charge efficiency.

η_{db} Mean battery discharge efficiency.

η_i Mean inverter efficiency.

η_M Mean electric motor efficiency of the pump.

η_P Mean pump efficiency

η_{pa} Mean power conditioner efficiency.

η_{pv} Mean photovoltaic array efficiency at Standard Test Conditions for both installations.

1. Introduction

Solar energy technologies for cooling applications have a high growth potential (Otanicar et al., 2012). In general, annual solar radiation profiles match better cooling demand profiles than heating demand profiles, because more cooling power is required when solar energy is abundant.

Due to the intermittent character of solar radiation and to the variations in the cooling demand during day and night, solar cooling technologies require energy storage systems or alternative energy sources to overcome the problem of meeting the cooling demand with the solar energy production.

The most widespread options of solar radiation use for cooling applications, are solar thermal driven adsorption, desiccant, absorption or solar mechanical compression system (Ge et al., 2018; Lazzarin and Noro, 2018; Palomba et al., 2019; Pintaldi et al., 2015; Sarbu and Sebarchievici, 2013) based on different solar collectors types operating in different temperature ranges: flat plate collector (FPC) (300 K–350 K), evacuated tube collector (ETC) (320 K–480 K), compound parabolic collector (CPC) (330 K–510 K), single-axis tracking Linear Fresnel reflector (LFR) (330 K–530 K), parabolic trough collector (PTC) (330 K–570 K) and cylindrical trough collector (CTC) (330–570 K) (Lillo-Bravo et al., 2018). In these applications, solar thermal energy is used to realize the regeneration of adsorbent/sorbent. The majority of these technologies require thermal energy storage (TES) systems to balance the cooling demand and the energy production. In many cases, the TES system uses a tank, which can be made of different materials (Alva et al., 2017). Frequently, the TES system is not included into the cooling cycle. The solar collector provides energy to the TES and the TES provides thermal energy to the cooling cycle. However, there are proposals to integrate the TES system into the cooling cycle. For instance, Xu et al. (2011) use a refrigerant storage tank into the absorption cooling cycle connected directly to the solar thermal collector using lithium bromide (H2O-LiBr) as the working fluid.

An alternative for solar cooling applications are photovoltaic (PV) systems used to power a conventional vapour compression cooling cycle. Cooling PV systems were limited by low PV efficiency and high initial investment; thus their application has been ignored until recent years. Nevertheless, cooling PV systems have a high thermodynamic potential (Lillo and Silva, 2014) and the electrical heat pumps are expected to provide heating and cooling with high efficiency (Chua et al., 2010), thanks to better components such as compressors (Ma and Zhao, 2008; Wang et al., 2009) and evaporators (Visek et al., 2014), and new configurations, integrated or not with renewable energy systems. In addition, due to the reduction of PV module and vapour-compression cycle equipment prices, this alternative is likely to attract more and more attention in the near future.

Batteries are the most commonly used energy storage system in stand-alone photovoltaic systems for cooling. For instance, Bilgili et al. (2011) and Torres-Toledo et al. (2016), include batteries that supply power to the compressor of the refrigeration cycle, thus ensuring the cooling demand when there is not sufficient solar radiation.

The efficiency of batteries varies as a result of highly diverse technology, fabrication materials, and industrial drivers (Shuru et al., 2018; Xu et al., 2018). There are important areas of research in batteries, from lines focused on controller systems (Awadallah and Venkatesh, 2016; Lv et al., 2016; Rajani and Pandya, 2016) to the development of new materials. (Arenas et al, 2017) and technologies (Khan et al., 2017). For instance, lead-acid batteries have seen efficiency improvements through carbon enhancement, which effectively combats self-discharge. Lithium ion batteries boast are improving with demands from the electric vehicle industry in rapid charge-discharge cycles. Despite this effort in research, today the cost of the battery storage of a photovoltaic system is very significant. Andreas Jossen et al. (2004) estimate that the cost of a storage system with lead-acid batteries can reach 50% of the cost of a stand-alone photovoltaic system. For this reason, the search for alternatives to batteries is of great interest.

Axaopoulos and Theodoridis (2009) propose, as an alternative to the use of batteries, the use of ice-water tanks as storage system using a specific controller for four compressors with photovoltaic panels and without batteries, however this solution requires solving some technological challenges such as compressors control and ice nucleation control, among others. Veerakumar and Sreekumar (2016) propose the use of phase change materials (PCMs) for refrigeration energy storage. Oró et al. (2012) review the PCMs for cold thermal energy storage applications, using a tank with PCM as an alternative to the ice tank. PCMs usually have low thermal conductivity and some of them such as eutectic salt solutions could be corrosive and chemically unstable. Another application of PCM in PV cooling processes is the one proposed by Fuqiao Wang et al. in their three-part study (Wang et al., 2007a, 2007b, 2007c). The authors propose incorporating PCMs in different positions inside the cooling cycle to improve the cycle efficiency, but not for ensuring the cooling demand.

Another possibility to ensure the cooling demand is the use of hybrid PV systems without an energy storage system. These systems compensate the photovoltaic electricity production with the electricity provided by another energy source according to the demand. For instance, for grid-connected PV applications, Fong et al. (2010) propose the combination of a PV system, without battery, connected in parallel with the electric grid for building air conditioning. Nowadays, there is commercial equipment in the market based on this combination (Frigicoll Company, 2014). Ozcan and Akyavuz (2017) propose a hybrid system, consisting of photovoltaic modules and fuel cells. Mira-Hernández et al. (2016) analyse a compressed-liquid energy storage with an adsorption-based vapour accumulator for solar-driven vapour compression systems in residential cooling. They highlight that, for the practical feasibility of the proposed configuration, the development of refrigerants with more favourable adsorption behaviour is required.

On the other hand, PV configurations, including photovoltaic panels inside the cooling production cycles, have also been developed. These systems, called solar assisted heat pumps (SAHP), are based on the use of direct-expansion solar collectors to replace the standard air source evaporator in a heat pump system. These configurations use different designs of hybrid photovoltaic/thermal (PV/T) panels (Alobaid et al., 2017; Beccali et al., 2009; Chen et al., 2011; Hu et al., 2010; Ji et al., 2008; Keliang et al., 2009; Saitoh et al., 2003; Xie et al., 2006). The purpose of these configurations is not to ensure the cooling demand but to increase the performance coefficient of the heat pump and to improve the performance of the PV panels

All of these studies highlight the interest in the search for new materials, technologies and configurations for cooling stand-alone photovoltaic installations.

This paper presents a novel storage system for cooling stand-alone photovoltaic installations. This system is based on using a thermally insulated tank closed with a moving plunger with ammonia in saturated mixture phase integrated into the vapour-compression cooling cycle. The tank is used as an energy storage system at constant pressure equal to the steam pressure of the refrigerant at the evaporator temperature. The aim of the paper is to describe the components of the novel system with all its operating modes. The installation is assessed in terms of Energy Efficiency Ratio (EER), required photovoltaic array area (A_{pv}), PV array energy (E_{pv}), total costs (C_t), tank volume (V_t) and refrigerant mass (m_{ref}) for three cooling applications: air conditioning with an evaporator temperature of 283 K, for food preservation with an evaporator temperature of 268 K and for freezing with an evapo- rator temperature of 250 K. To this end, all these technical variables have been calculated to supply 1 kW-hour of cooling production for one day on a site characterized by an average daily solar radiation on the PV module plane of 5 kWh/m^2·day with a condenser tem- perature (or ambient temperature) from 283 K to 313 K. In addition, the required photovoltaic array area and the total costs of this configuration is compared, on the same terms, with the most frequent PV configuration for cooling production: a PV array, a battery (as the storage system) and an inverter, connected to a conventional vapour-compression cooling cycle. The battery energy capacity (E_b), E_{pv} and EER are also analysed for this configuration.

The structure of the paper is as follows: in Section 2, the proposed photovoltaic installation for cooling production is described and its operating modes are defined in detail. In Section 3, the photovoltaic installation used as a reference is described. In Section 4, the methodology followed to analyse the PV installation proposed is presented. In Section 5, the size of the components, the efficiency and the cost of both installations are assessed by cooling demand unit. The main conclusions of this study are outlined in Section 6.

2. Description of the proposed installation

Fig. 1 shows the proposed stand-alone photovoltaic installation for cooling production called installation 1. This installation uses the excess available PV electricity during low or null cooling demand periods to compress additional refrigerant vapour, which is condensed, expanded and stored at constant pressure so it can be evaporated at a later time when the cooling demand cannot be met with the available electricity.

The proposed installation consists of a PV array connected to the compressor through a power conditioning system or inverter. The vapour-compression cooling cycle includes a pressurized and thermally insulated storage tank (ST), with ammonia (R717) as refrigerant in saturated mixture phase, connected to the expansion valve outlet (Fig. 1, point 8), to the three-way valve inlet (Fig. 1, point 10) and to the pump inlet (Fig. 1, point 9). The pump is powered by an auxiliary battery. All other components are the same as those of a conventional vapour-compression cooling cycle.

This configuration is similar to the used by Xu et al. (2011), but in the present proposal the tank is integrated into a compression cycle, not into an absorption cycle, and the refrigerant is ammonia instead of lithium bromide (H2O-LiBr). In addition, this configuration is suitable to different evaporator temperatures (250 K, 268 K and 283 K) and applications, whereas Xu's proposal is only applied to air conditioning applications.

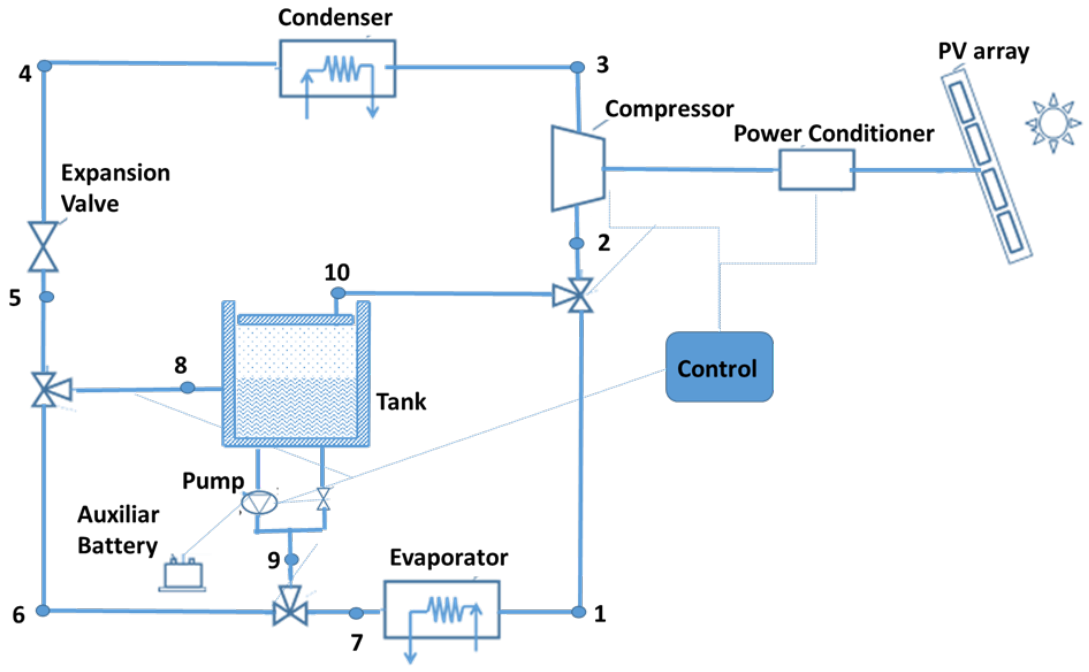

Fig. 1. Proposed installation 1.

2.1. Operating modes

The proposed installation 1 has five operating modes. Figure 2 shows five diagrams, from"a" to" e" that correspond to each operation mode from 1 to 5 respectively.. In these diagrams, the red solid lines show where the refrigerant is running in each operating mode and the arrows show their flow direction. Moreover, when the PV array powers the compressor for cooling production the dotted line which joins both systems is depicted in red. The five operating modes are described in detail bellow:

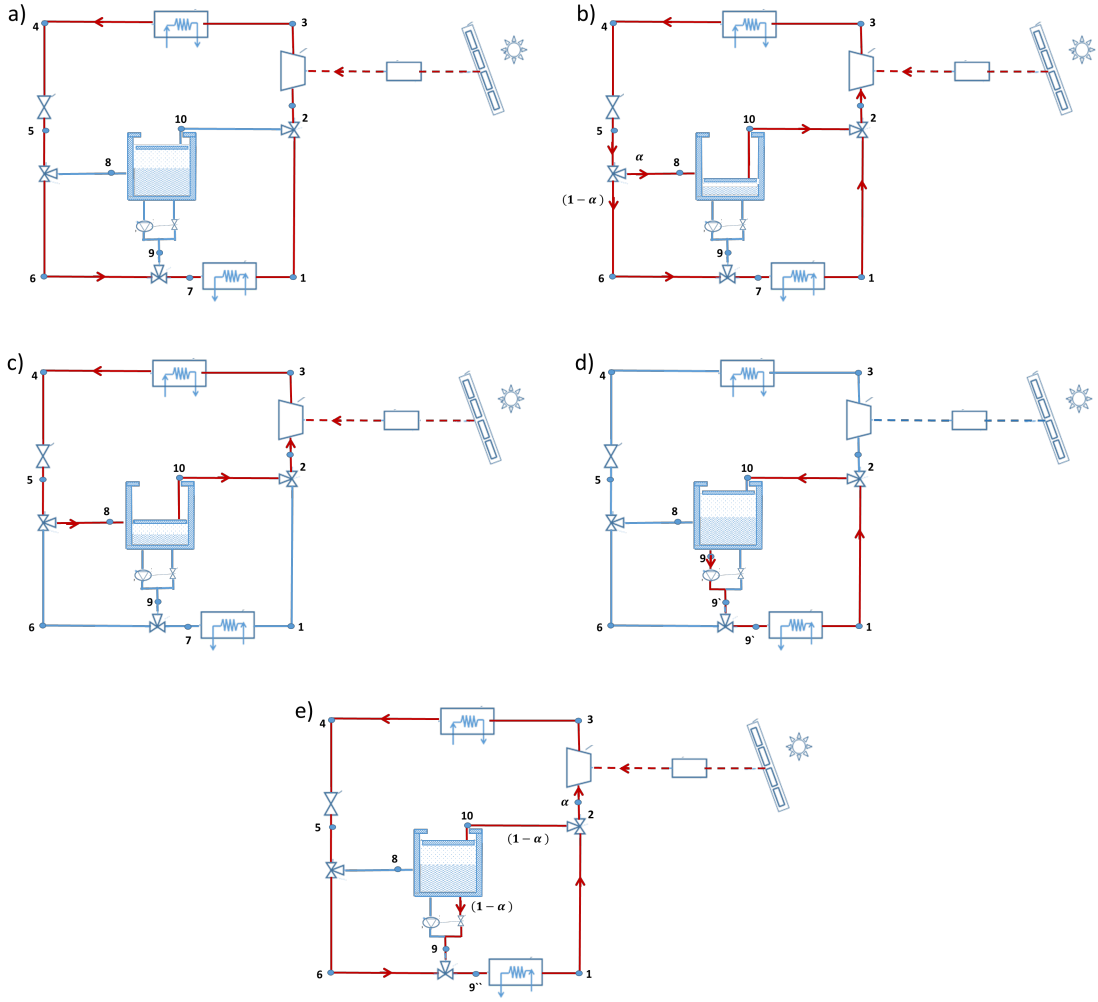

Fig. 2. Installation 1 operating modes: a) operating mode 1, b) operating mode 2, c) operating mode 3, d) operating mode 4 and e) operating mode 5.

Operating mode 1 (Fig. 2a): This operation mode corresponds to cooling production from only PV array, the energy storage is inactive. The vapour-compression cooling cycle is exclusively powered from the PV array; the energy storage tank remains inactive. In this case, the PV array powers the compressor for cooling production, without variation of the steam quality of the refrigerant stored in the tank. This operating mode is used when the available electricity exactly matches the cooling demand.

In this operation mode, the Installation 1 produces cold according to the compressor operating conditions, which in turn depends on the electrical production of the PV array as a function of the available solar radiation and the condenser and evaporator temperatures, according to the p-h diagram shown in Fig 3. Tank volume is constant during this operating mode as it is shown in Fig. 3.

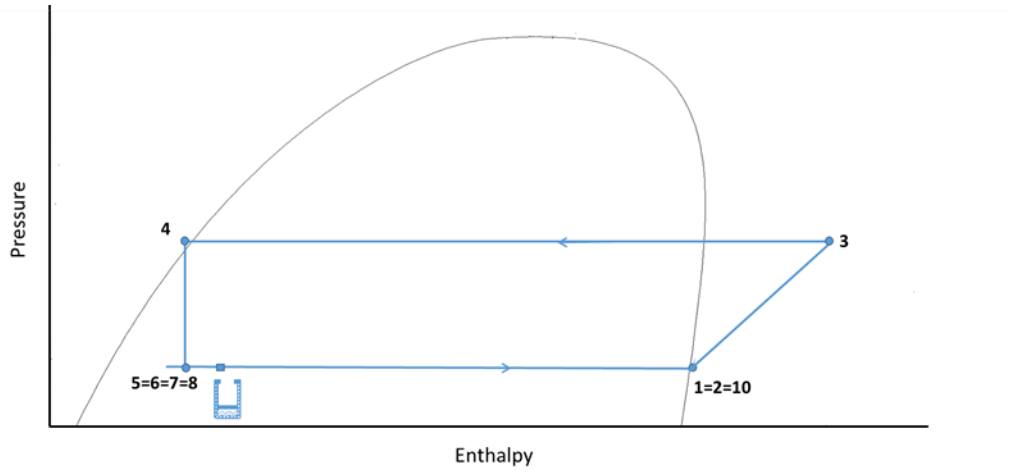

Fig 3. p-h diagram of the operating mode 1. During this mode the tank volume and refrigerant vapour quality in the tank is constant.

Operating mode 2 (Fig. 2b): This operation mode corresponds to cooling production and energy storage charge. The vapour-compression cooling cycle is operated to produce cooling and to increase the energy stored in the tank, by reducing the refrigerant vapour quality. According to Fig. 4, as the refrigerant flow exits the valve (point 5), a fraction α of the liquid refrigerant enters in the tank (point 8) and the other refrigerant fraction, 1-α, flows through the evaporator (points 6-7). The refrigerant circulates from the evaporator outlet (point 1) together with saturated vapour from the tank outlet (point 10) through the compressor and condenser, and returns to the expansion valve inlet, according to the p-h diagram shown in Fig 4. Tank volume and refrigerant vapour quality in the tank are decreasing during this operating mode, as it is shown in Fig.4.(thick arrow).

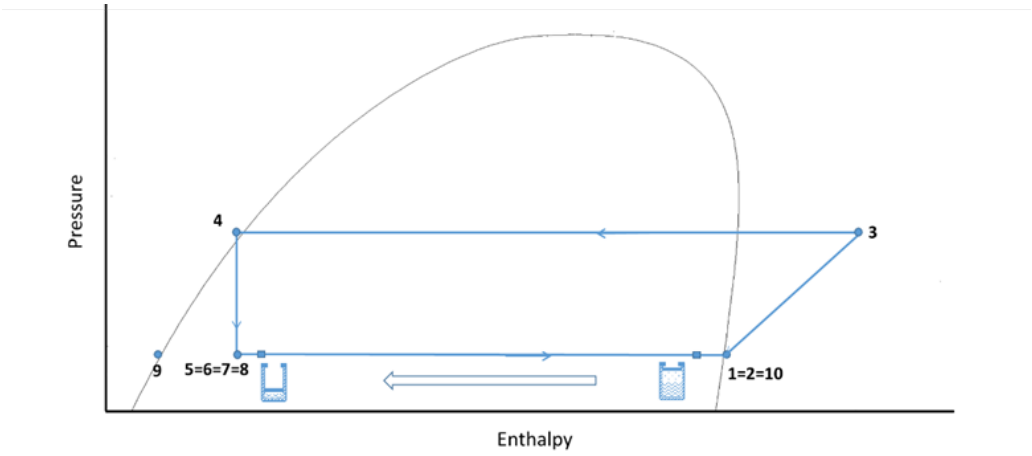

Fig 4. p-h diagram of the operating mode 2. During this mode decreases the tank volume and refrigerant vapour quality in the tank.

This operating mode is used when there is an excess of available electricity to meet the cooling demand. The installation 1 produces cold according to the cooling demand but the cooling cycle can decrease the refrigerant vapour quality in the tank, recirculating the refrigerant from the tank by means of the compressor, thereby increasing the storage capacity. As the refrigerant vapour quality in the tank decreases, the installation storage capacity increases.

Operating mode 3 (Fig. 2c): This operation mode is used when there is available electricity to drive the compressor but there is no cooling demand. This operation mode exclusively increases the energy stored in the tank. The vapour-compression cooling cycle is operated reducing the refrigerant vapour quality in the tank without cooling production, according to the p-h diagram shown in Fig 5. The tank volume and refrigerant vapour quality in the tank are decrease during this operating mode, as shown in Fig. 5.(thick arrow).

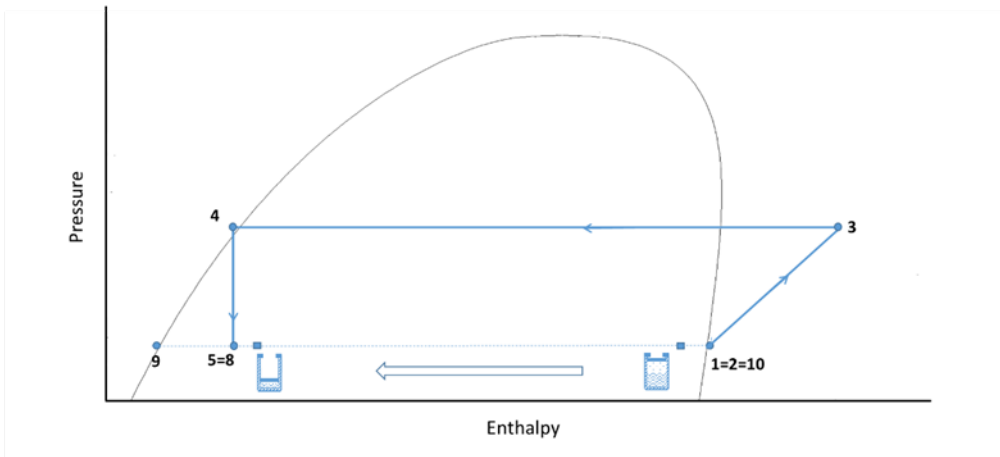

Fig 5. p-h diagram of the operating mode 3. During this mode decreases the tank volume and refrigerant vapour quality in the tank.

Operating mode 4 (Fig. 2d): This operation mode corresponds to cooling production exclusively from storage; energy storage discharge. The vapour-compression cycle produces cooling from the energy stored in the storage tank, increasing the refrigerant vapour quality in the tank, according to the p-h diagram shown in Fig 6. Tank volume and refrigerant vapour quality are increasing during this operating mode. The compressor does not work. According to Fig. 6, the refrigerant exits the tank in saturated liquid phase (point 9) and enters into the evaporator at point 7. The refrigerant returns to the tank (point 10 from the evaporator outlet (point 1)) while the compressor does not work.

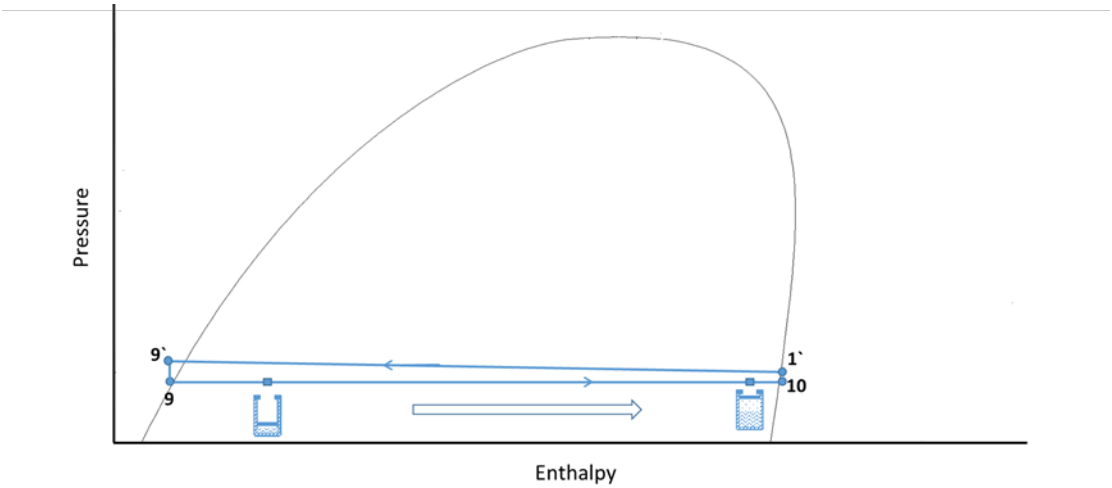

Fig 6. p-h diagram of the operating mode 4. During this mode increases the tank volume and refrigerant vapour quality in the tank.

Operating mode 5 (Fig. 2e): This operation mode corresponds to cooling production from PV and energy storage; energy storage discharge. A fraction α of the refrigerant flow entering the three-way valve (point 1) goes to the compressor (point 2) and the other refrigerant fraction, 1-α, goes to the tank (point 10); the refrigerant fraction 1-α leaves the tank as saturated liquid (point 9) and together with the refrigerant fraction α, from the expansion valve (point 6) reach the point 9`` at the evaporator input, according to the p-h diagram shown in Fig 7. The tank refrigerant vapour quality and tank volume increase.

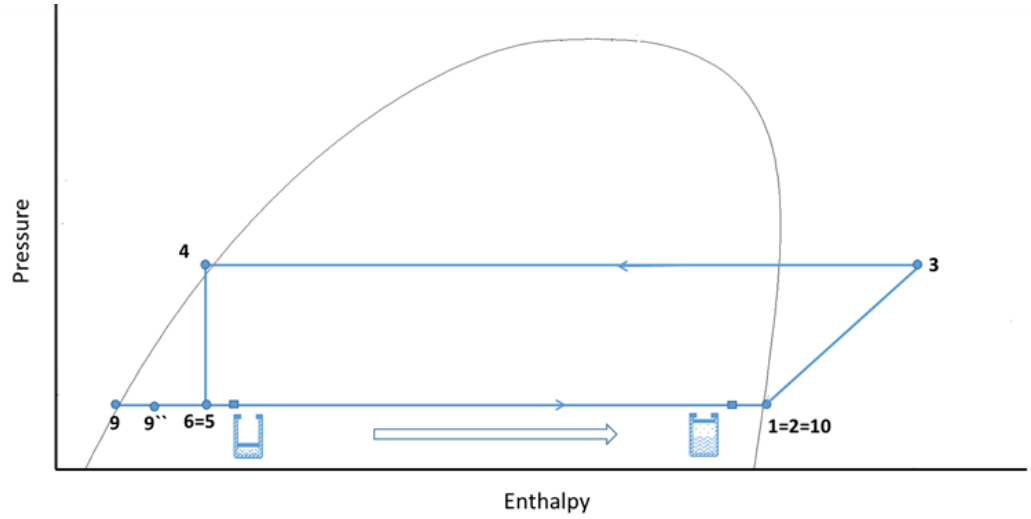

Fig 7. p-h diagram of the operating mode 5. During this mode increases the tank volume and refrigerant vapour quality in the tank.

This operating mode is used when the available electricity is insufficient to meet the cooling demand. The saturated liquid is discharged from the tank to assist in providing the required cooling demand. The compressor operating conditions depend on the PV electricity production according to climatic conditions. The tank complements the refrigerant flow from the compressor to provide the cooling demand.

The potential issues related to the control of the installation in the different operating modes must be analysed and solved but are out of the scope of the current work.

3. **Description of the reference installation**

Fig. 8 shows a stand-alone photovoltaic installation with battery for cooling production. This installation, called installation 2, is used as reference. Installation 2 consists of a PV array, with a battery (B) as energy storage system, with a charge controller and inverter that powers the compressor of a conventional vapour-compression cooling cycle. This installation has the possibility to provide cooling at times when there is not sufficient available electricity thanks to the energy stored in the battery.

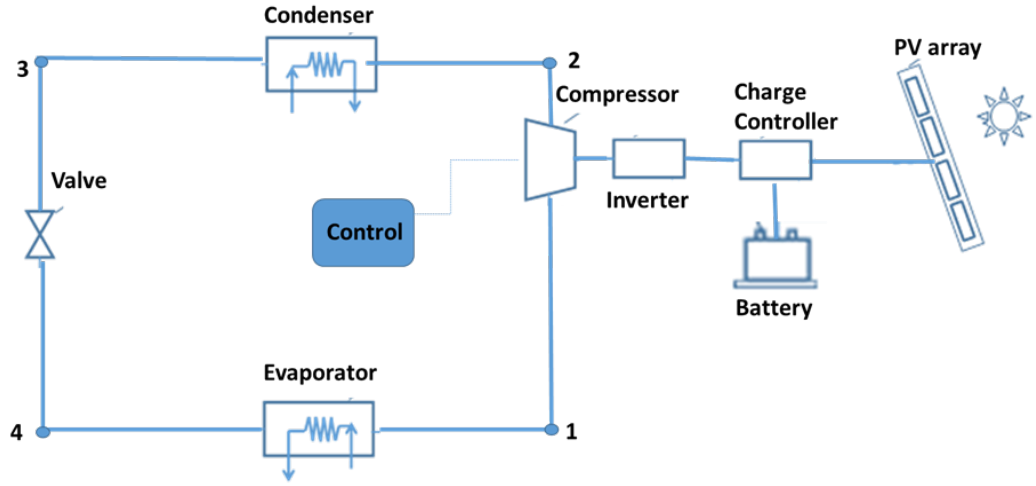

Fig. 8. Reference installation 2.

For both installations, ammonia has been selected as refrigerant due to its wide range of operating temperatures (223K-288K), low cost, excellent thermodynamic properties leading to a high EER, low specific volume in the saturated vapour phase compared to other refrigerants, minimal environmental impact, zero Ozone Depletion Potential and zero Global Warming Potential (34-2007 (Standard ANSI/ASHRAE), 2007). According to the ASHRAE classification (34-2007 (Standard ANSI/ASHRAE), 2007), ammonia belongs to the B2L safety group, with low flammability but toxic and corrosive features, thus requiring appropriate safety controls.

4. Methodology

Installation 1 and Installation 2 are assessed for the three cooling applications in terms of Energy Efficiency Ratio (EER), required photovoltaic array area (A_{pv}),total costs (C_t), tank volume (V_t) and refrigerant mass (m_{ref}) of Installation 1 and the energy capacity of the battery B, (E_b) of Installation 2. To this end, all these technical variables have been calculated per kilowatt-hour unit of cooling capacity, for three evaporator temperatures depending on the cooling use, 283 K for air conditioning, 268 K for food preservation and 250 K for freezing. This comparison is addressed for a site characterized by an average daily solar radiation on the PV module plane of 5 kWh /m^2·day with a condenser temperature from 283 K to 313 K.

The cooling effect produced by the evaporator of the Installation 1, (Q_L), is determined by Eq. (1):

$$Q_L = m_{ref} \cdot (h_1 - h_7)/3600 \quad (1)$$

where h_1 is the specific enthalpy at the point 1 and h_7 at the point 7. The specific enthalpy of all points are calculated using the Refprop software (Lemmon et al., 2002). The cooling cycle model has been implemented and simulated with the Engineering Equation Solver (EES) software

(Klein, 1992). The required refrigerant mass, (m_{ref}) to provide a cooling demand Q_L equal to 1 kWhc is determined by Eq. (2):

$$m_{ref} = 3600\ /(h_1 - h_7) \tag{2}$$

The required pumping power (P) to overcome the pressure drop in the hydraulic circuit from point 9 to point 10 is determined by Eq. (3) :

$$P_p = (\rho_9 \cdot g \cdot q_{v9} \cdot H_p)\ /\eta_M \cdot \eta_p \tag{3}$$

where $q_{V9}(\frac{m3}{s})$ is the refrigerant volumetric flow in point 9, ρ_9 (kg/m^3) is the ammonia density at point 9, g (m/s^2) is the acceleration of gravity and H_p (m of water column) is the pressure drop in the cooling circuit between point 9 and point 10 according to Fig. 1.

The required auxiliary battery energy (E_{Baux}) to drive the pump P is determined by Eq. (4):

$$E_{Baux} = (g \cdot m_{ref} \cdot H_P)\ /(\eta_M \cdot \eta_P \cdot \eta_{db} \cdot DoD) \tag{4}$$

where η_M is the efficiency of the electric motor of the pump, η_p is the pump efficiency, η_{db} is the battery efficiency and DoD is the battery depth of discharge.

The EER$_1$ and the compressor energy consumption of the installation 1, (E_{c1}) expressed in kWh, for a cooling demand of $Q_L$equal to 1 $kWhc/d$ is expressed as:

$$EER_1 = \frac{Q_L}{E_{c1}} = \frac{1\ kWh}{E_{c1}} = \frac{(h_1 - h_7)}{(h_3 - h_2)} \tag{5}$$

where E_{c1} is the compressor required energy of the installation 1, calculated according to Eq.(6).

$$E_{c1} = \frac{(h_3 - h_2)}{(h_1 - h_7)} \cdot 1\ kWh \tag{6}$$

The required energy at the output of the solar field of the installation 1 (E_{pv1}) is calculated by the Eq. (7):

$$E_{pv1} = \frac{E_{c1}}{\eta_{pa}} \tag{7}$$

where η_{pa} is the power conditioner efficiency.

The required solar array area of Installation 1, (A_{pv1}) is calculated by Eq. (8):

$$A_{pv1} = \frac{E_{pv1}}{\eta_{pv} \cdot H_G} \tag{8}$$

where η_{pv} is the PV array efficiency at Standard Test Conditions (1000 W/m^2, 25ºC, AM=1,5), and H_G is the daily total solar radiation on the PV module plane (kWh /m^2·d).

The energy at the output of the solar array (E_{pv2}) required to cover the compressor energy demand of Installation 2, (E_{c2}), is calculated by the Eq. (9):

$$E_{pv2} = \frac{E_{c2}}{\eta_{cb} \cdot \eta_{db} \cdot \eta_i} \tag{9}$$

and the compressor energy demand of the installation 2, (E_{c2}), according to Fig. 2, is calculated by Eq. (10):

$$E_{c2} = \frac{(h_2 - h_1)}{(h_1 - h_4)} \cdot 1 \text{ kWh} \qquad \text{with} \qquad EER_2 = \frac{1 \text{ kWhc}}{E_{c2}} \tag{10}$$

The required solar array area of the installation 2 is calculated by Eq. (11):

$$A_{pv2} = \frac{E_{pv2}}{\eta_{pv} \cdot H_G} \tag{11}$$

The tank volume changes according to the refrigerant conditions to keep the refrigerant at constant pressure. The pressure in the tank is the steam pressure of the refrigerant at the evaporator temperature. The required maximum refrigerant tank volume V_t, per cooling unit (kWhc), in the installation 2 is calculated by Eq. (12):

$$V_t = 1{,}15 \cdot m_{ref} \cdot v_{ref}(p_1) \tag{12}$$

where 15% of additional volume is included as a security margin; $v_{ref}(p_1)$ is the refrigerant specific volume (m^3/kg) at the evaporator outlet, point 1.

The minimum pressure that the tank has to stand (p_T) is calculated as 1.5 times the steam pressure of the refrigerant at the evaporator temperature, $p^{f+g}(T_{ev})$ according to Eq. (13).

$$p_T = 1{,}5 \cdot p^{f+g}(T_{ev}) \tag{13}$$

The battery size, E_b of installation 2, in kWh, is calculated by Eq. (14):

$$E_b = \frac{E_{c2}}{\eta_{db} \cdot \eta_{i \cdot DoD}} \tag{14}$$

The total costs for both installations are determined by Eqs. (15) and (16):

$$C_{t1} = A_{pv1} \cdot P_{sa} + V_t \cdot P_t + m_{ref} \cdot P_{ref} \cdot \left(1 + \frac{1}{(1+r)^{\text{tr}}}\right) \tag{15}$$

$$C_{t2} = A_{pv2} \cdot P_{sa} + E_b \cdot P_b \cdot \left(1 + \frac{1}{(1+r)^{\text{tb1}}} + \frac{1}{(1+r)^{\text{tb2}}}\right) \tag{16}$$

where C_{t1} is the installation 1 total cost (excluding the cooling cycle costs except the refrigerant and the tank) (€/kWhc), C_{t2} the installation 2 total cost (excluding the cooling cycle costs) (€/kWhc), P_t the refrigerant tank cost (€/m^3), P_b the battery cost per storage kWh (€/kWh), P_{sa} the PV array cost (€/m^2), P_{ref} the refrigerant cost (€/kg), r the annual discount rate, %, tb_1 and

tb_2 are the period in years of reposition of the battery, and *tr* is the period, in years, of reposition of the refrigerant. The comparison between the two installations has been made under the following assumptions:

1.- Analysis period for both installations: 30 years.

2.- The PV array consists of monocrystalline silicon modules that work in Standard Test Conditions (STC). The PV array efficiency (η_{pv}) is 15% for both installations with a lifetime of 30 years (Sampaio and González, 2017).

3.- The depth of discharge of the battery (DoD) is 75 % with average charge efficiency (η_{cb}) and average battery discharge efficiency (η_{db}) of 80 % (Bruch and Müller, 2014). The useful life of the battery is 10 years (Rajani and Pandya, 2016), so it should be replaced 2 times during the analysis period, sotb1=10 and tb2=20.The discharge time for the purpose of calculating the required energy capacity of the battery E_b is 10 h . The average inverter efficiency,η_i, the average power conditioner efficiency, η_{pa} and the average pump electric motor efficiency, η_M,are 90 % (Onur and Ugur Sava, 2011). The average auxiliary pump hydraulic efficiency η_P is 70 %. A useful life of 30 years is considered for the inverter, charge controller, power conditioner, motor and pump; the isentropic efficiency the compression process is 75%.

4.- The useful life of the ammonia refrigerant is 15 years, so it should be replaced once during the analysed period, so tr=15. The proposed tank should have an internal coating of stainless steel reinforced with fiber or polyester on the outside. The tank volume has been increased by 15% as a safety margin with respect to the theoretical minimum required volume. The useful life of the tank is 30 years.

5.- In both installations, the heat pump operation and maintenance costs are considered equal and they have not been included in the comparative analysis.

6.- The incidence of the recirculation pump and the auxiliary battery required in the installation 1 are neglected in the economic calculations and energy balances.

7.- The storage tank and valves operate adiabatically. The evaporator and condenser operate at constant pressure. The mass flow of the incoming streams to the condenser is controlled by a control system as a function of the power input to the compressor available from the PV system and the cooling demand.

8.- It is assumed that the refrigerant phase is saturated vapour at the evaporator outlet and upper storage tank outlet (point 10), superheated vapour at the compressor outlet, saturated liquid at the condenser outlet and lower storage tank outlet (point 9) and saturated mixture at the expansion

valve outlet and inside the storage tank. The vapour-compression cooling cycle devices are modelled as steady-state to get a cooling demand of 1 kWhc.

9.- For the economic comparison, a discount rate value (r) of 3 %/year is assumed for both installations. The equipment costs and the sensitivity range shown in Table 1 are assumed for the calculation of the total costs of both installations.

Table 1. Price of main components.

	Cost	Sensitivity Range	References
Tank	P_t= 400€/m^3	200-1000 €/m^3	(*)
Battery	P_b= 250 €/kWh.	100-500 €/kWh	(Bruch and Müller, 2014; Onur and Ugur Sava, 2011; "Solaray energy," 2013)
PV Array	P_{sa}=1,5 €/Wp.	1-2,5 €/Wp.	("PV-magazine," 2016) (**)
Refrigerant	P_{ref}= 2 €/kg	-	("Market realist," 2016)

(*) Prices contributed by several companies in Spain.
(**) Assuming 160 Wp/m^2.

5. Results and discussion

Figs. 9, 10 and 11 represent tank volume, refrigerant mass, PV array energy, and Energy Efficiency Ratio, respectively, as a function of the condenser temperature (T_D) for the three evaporator temperatures (T_e) in Installation 1.

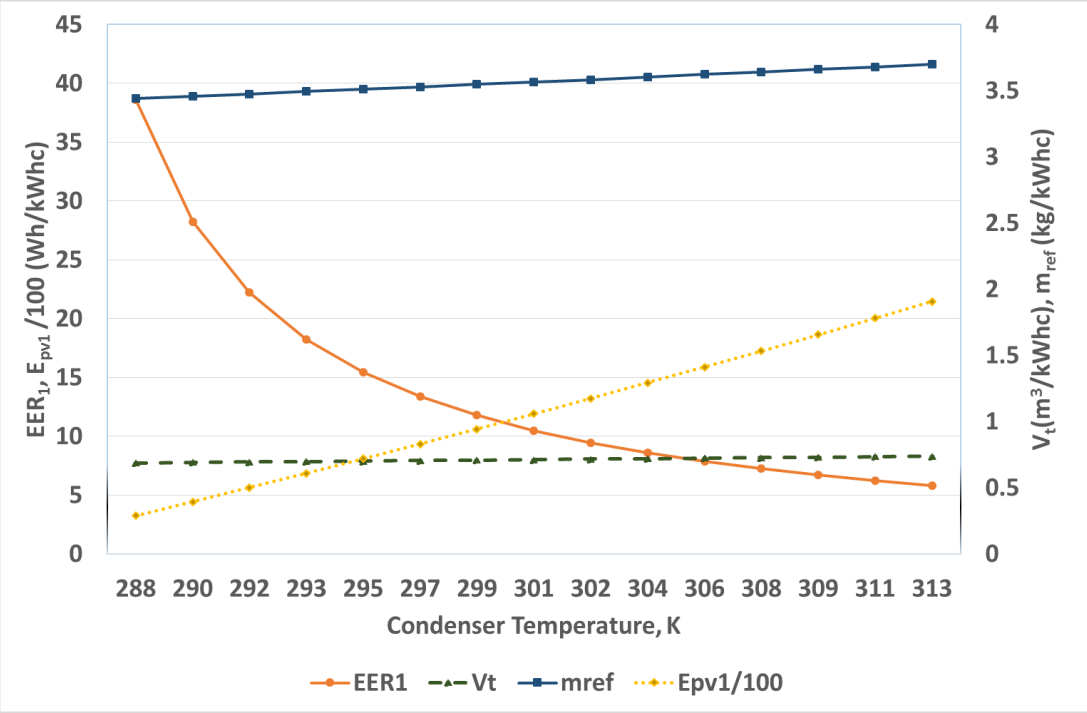

Fig. 9. Tank volume, refrigerant mass, PV array energy, and Energy Efficiency Ratio, for installation 1 depending on the condenser temperature for an evaporator temperature of 283 K.

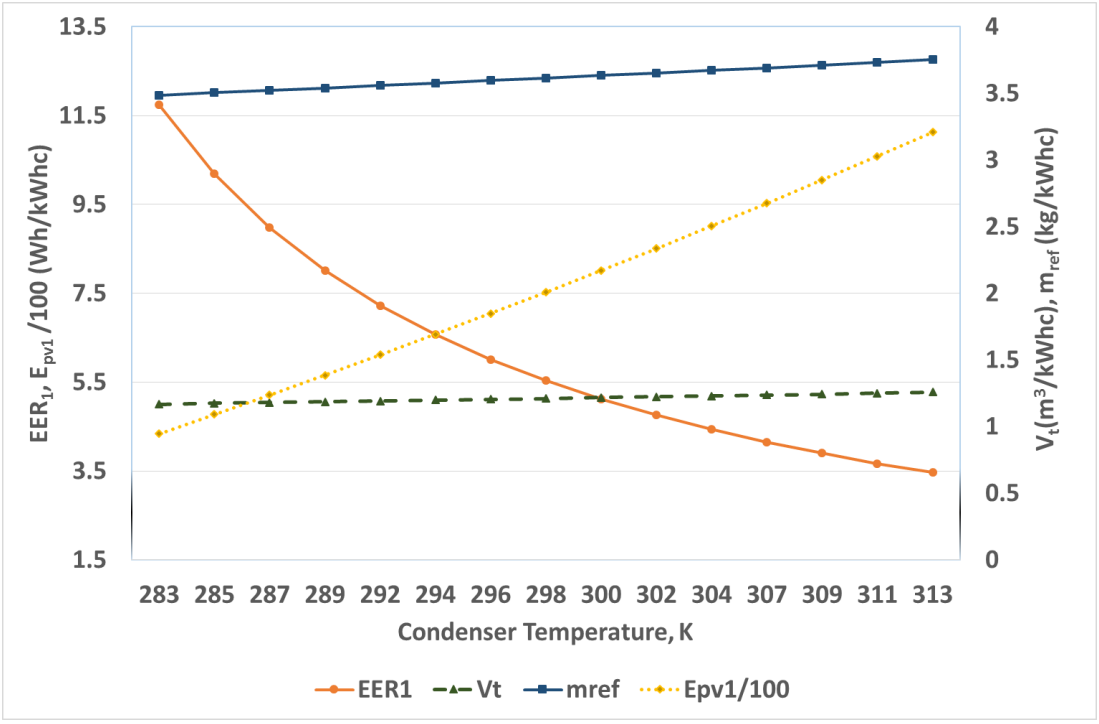

Fig. 10. Tank volume, refrigerant mass, PV array energy, and Energy Efficiency Ratio, for installation 1 depending on the condenser temperature for an evaporator temperature of 268 K.

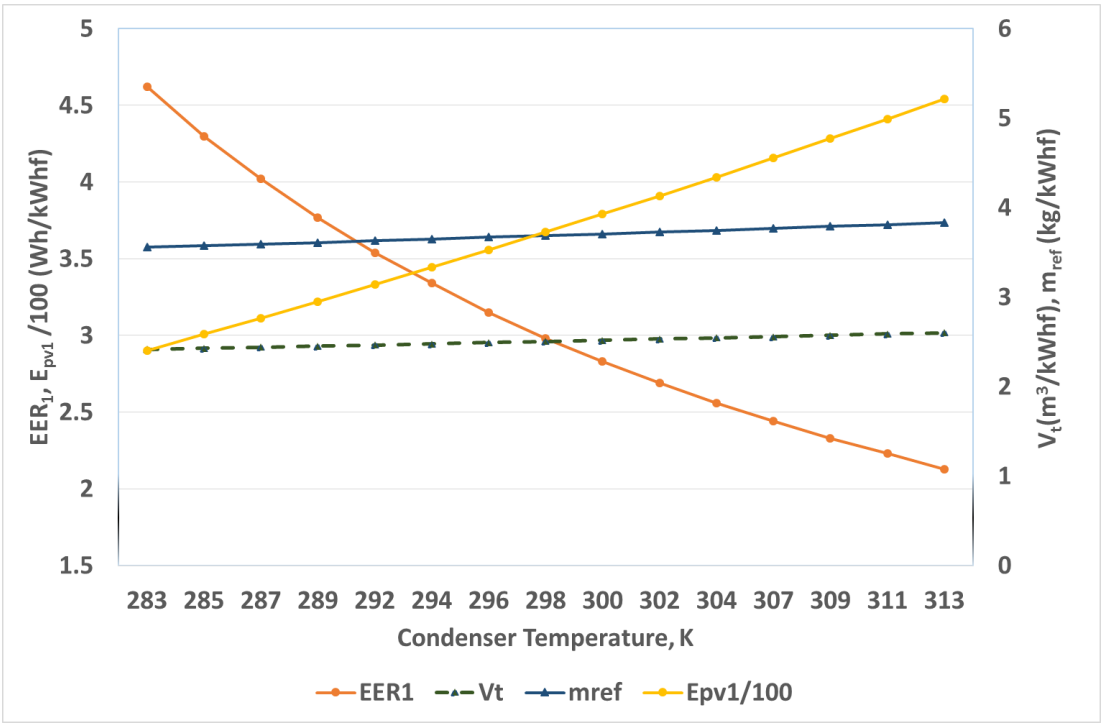

Fig. 11. Tank volume, refrigerant mass, PV array energy, and Energy Efficiency Ratio, for installation 1 depending on the condenser temperature for an evaporator temperature of 250 K.

The tank volume and the refrigerant mass vary significantly by varying the evaporator temperature. However, they vary slightly with condenser temperature. On the other hand, the

energy efficiency ratio and photovoltaic area vary significantly with both the evaporator and condenser temperatures.

For example, for a condenser temperature of 313 K, the tank volume, according to Eq. (12), is 2.6 m^3/kWhc and 0.7 m^3/kWhc for evaporator temperatures of 250 K and 283 K respectively. This is explained because the specific volume of the refrigerant in the state of saturated steam for a temperature of 283 K is 0.2 m^3/kg; while for a temperature of 250 K is 0.7 m^3/kg. The higher the evaporator temperature, the lower the tank volume is.

As shown in Figs 9, 10 and 11, the required refrigerant mass varies between 3.44 kg/kWhc and 3.83 kg/kWhc, increasing very slightly when the condenser temperature increases and the evaporator temperature decreases. For instance, for the same condenser temperature of 313 K, the required refrigerant mass are 3.8 kg/kWhc and 3.7 kg/kWhc for evaporator temperatures of 250 K and 283 K respectively.

According to Eq. (13), the pressure to be supported by the tank is proportional to the refrigerant vapour pressure at the evaporator outlet depending on the evaporator temperature. For example, the tank must withstand a minimum pressure of 918 kPa for an evaporator temperature of 283 K, 529 kPa for 268 K and 247 kPa for 250 K. The lower the evaporator temperature, the lower the maximum pressure the tank must withstand.

The required auxiliary pump power of Installation 1, P, is less than 2 W/kWhc and the size of the auxiliary battery E_{Baux} is less than 3 Wh/kWhc according to Eqs. (3) and (4), for a refrigerant flow rate of 1 g/s and a gauge height of 1.8 mwc. That is why it has been despised in the comparative analysis.

Figs. 12, 13 and 14 show the evolution of the battery energy capacity, E_b, the energy to be supplied by the solar field, E_{pv2}, and energy efficiency ratio, EER_2, of Installation 2 as a function of the condenser temperature for three evaporator temperatures, 283 K, 268 K and 250 K respectively.

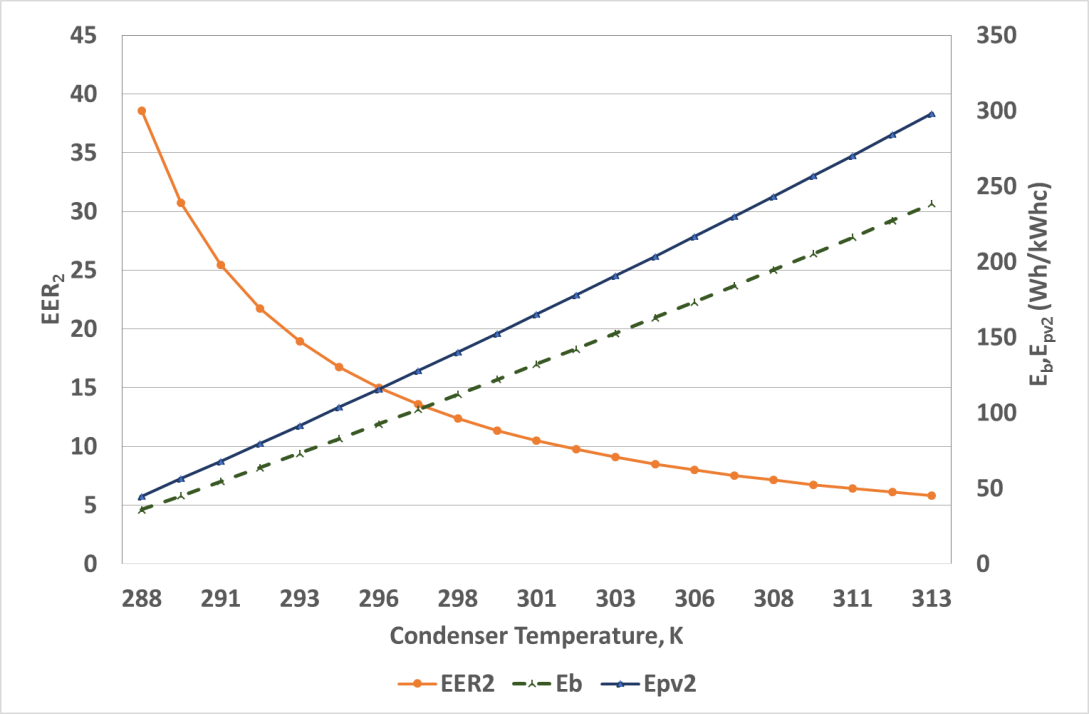

Fig. 12. Battery energy capacity, PV array energy, and energy efficiency ratio for installation 2 depending on the condenser temperature for an evaporator temperature of 283 K.

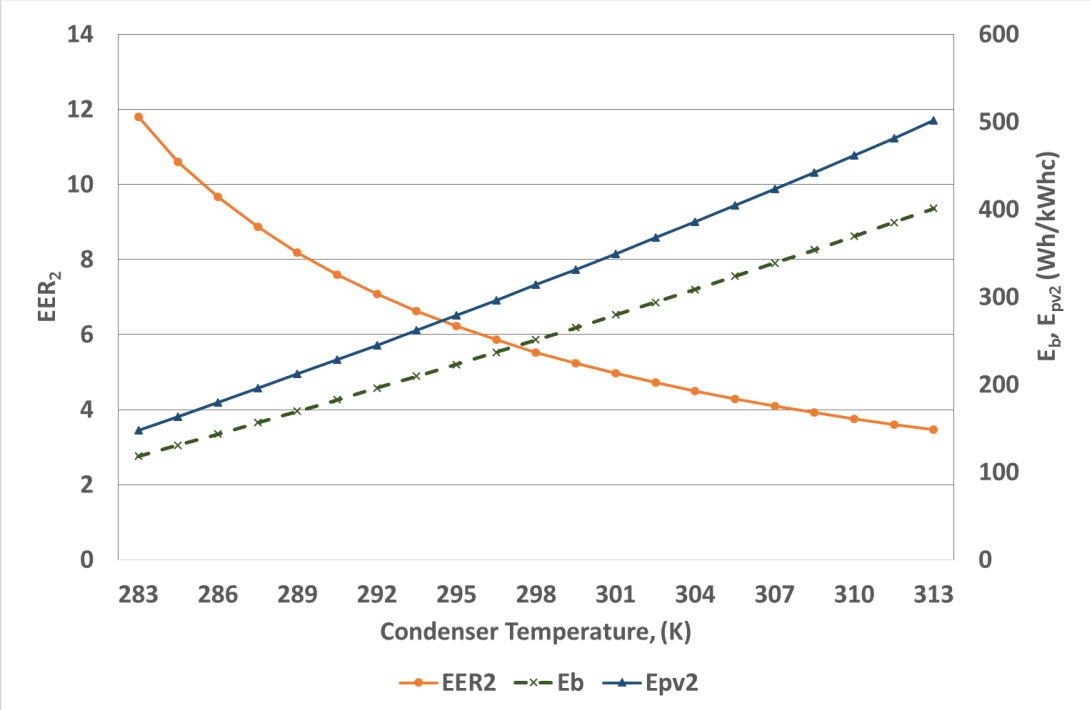

Fig. 13. Battery energy capacity, PV array energy, and energy efficiency ratio for installation 2 depending on the condenser temperature for an evaporator temperature of 268 K.

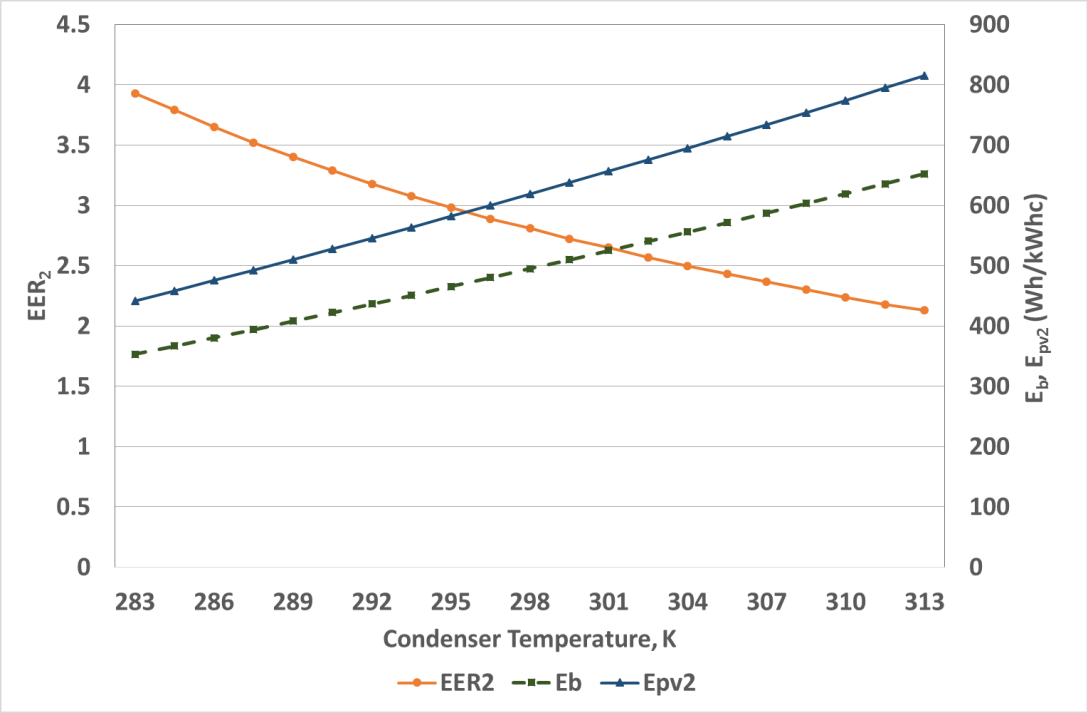

Fig. 14. Battery energy capacity, PV array energy, and energy efficiency ratio for installation 2 depending on the condenser temperature for an evaporator temperature of 250 K.

According to figures 12, 13 and 14, the battery energy capacity E_b increases almost linearly as the condenser temperature increases and the evaporator temperature decreases. For instance, for an evaporator temperature of 283 K, the size of the required battery is 51 Wh/kWhc for a condenser temperature of 288 K and 341 Wh/kWhc for a condenser temperature of 313 K. For an evaporator temperature of 250 K, and condenser temperatures of 288 K and 313 K the respective sizes are 505 Wh/kWhc and 932 Wh/kWhc.

Fig. 15 shows the required PV array area for both installations as a function of the condenser temperature for the three evaporator temperatures, 283 K, 268 K and 250 K.

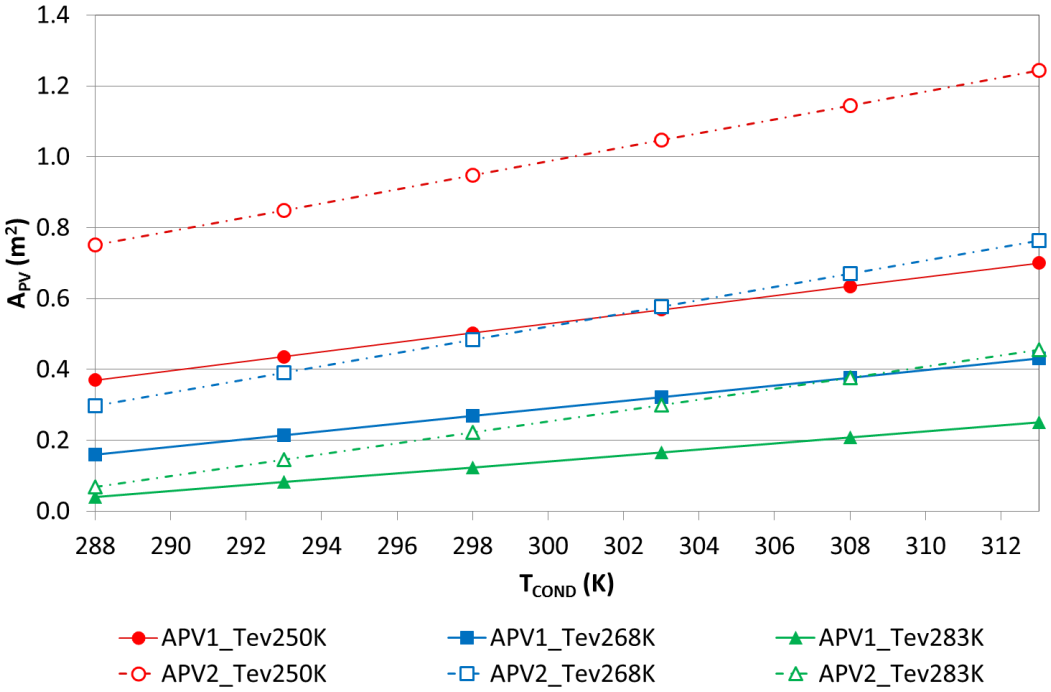

Fig. 15. Required PV array area for installations 1 and 2, as a function of condenser temperature for three evaporator temperatures.

The required PV area for installation 2 (A_{pv2}) is slightly higher than the required PV area for installation 1 (A_{pv1}) due mainly to the battery inefficiencies in the charging and discharging processes. The required PV area depends very strongly on the condenser and evaporator temperatures. These temperatures affect directly the cycle efficiency and therefore the electric energy required by the compressor. For a condenser temperature of 313 K and for evaporator temperatures of 250 K and 288 K, the required PV array areas (A_{pv1}) are 0,72 m^2/ kWhc and 0,23 m^2/kWhc respectively for Installation 1, while the required PV array area (A_{pv2}) are 1,24 m^2/ kWhc and 0,41 m^2/kWhc respectively for Installation 2. When the condenser temperature decreases, the required PV array area decreases. For instance, for a condenser temperature of 288 K, and evaporator temperatures of 250 K and 283 K, the required areas for Installation 1 are 0,38 m^2/ kWhc and 0,04 m^2/ kWhc respectively.

Fig. 16 shows the results of the total cost ratio, C_{t2}/C_{t1}, of both installations according to Eqs. (10) and (11) for the three evaporator temperatures considered 283 K, 268 K and 250 K and two condenser temperatures, 313 K y 293 K and a PV array cost of 1,5 €/Wp. (240 €/m^2).

T_e	Condenser temperature	
	293 K	313 K

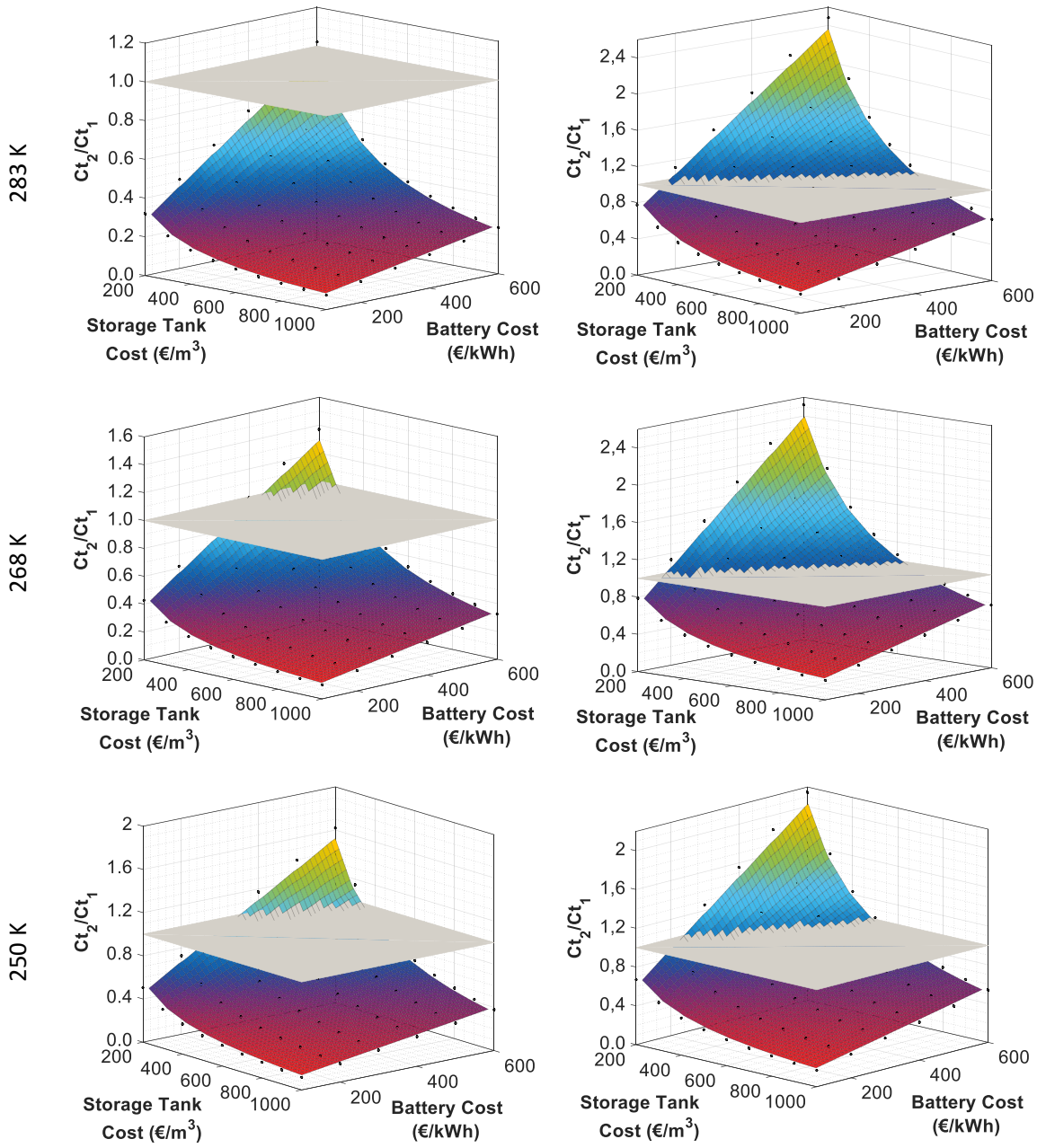

Fig 16. Total cost ratio, C_{t2}/C_{t1}, for two condenser temperatures, 293 K (left side) and 313 K (right side), and three evaporator temperature, 283 K (row 1), 268 K (row 2) and 250 K (row 3), for an PV array cost of 1,5 €/Wp. The grey plane indicates both installations have the same costs.

According to Fig. 16, the total costs of Installation 1 tend to be lower than those for Installation 2 as the price of the tank decreases and the price of the battery increases, in all cases. As the temperature of the evaporator decreases and the temperature of the condenser increases, the Installation 1 presents less total cost than Installation 2.

For air-conditioning applications with a T_e of 283 K and for condenser temperature of 293 K, with battery cost higher than 600 €/kWh and tank cost lower than 200 €/m^3, Installation 1 has lower total cost than Installation 2. For a condenser temperature of 313 K, the total cost of Installation 1 is lower when the tank cost (in €/m^3) is similar to or lower than the battery cost (in €/kWh).

For food preservation applications, with a T_e of 268 K and a condenser temperature of 293 K, with a battery cost higher than 400 €/kWh and tank cost lower than 200 €/m^3, Installation 1 has lower total cost than Installation 2. As in the previous case, for a condenser temperature of 313 K, the total cost of Installation 1 is lower when the tank cost (in €/m^3) is similar to or lower than the battery cost (in €/kWh).

For freezing applications, with a T_e of 250 K and a condenser temperature of 293 K, with a battery cost higher than 350 €/kWh and a tank cost lower than 300 €/m^3, Installation 1 has lower total cost than Installation 2. For a condenser temperature of 313 K, the total cost of Installation 1 is lower when the tank cost (in €/m^3) is lower than 90% of the battery cost (in €/kWh).

Fig. 17 shows the influence of the PV array cost for different tank cost (P_t) and a battery cost of 250 €/kWh in the cost ratio C_{t2}/C_{t1}, for an evaporator temperature of 283 K.

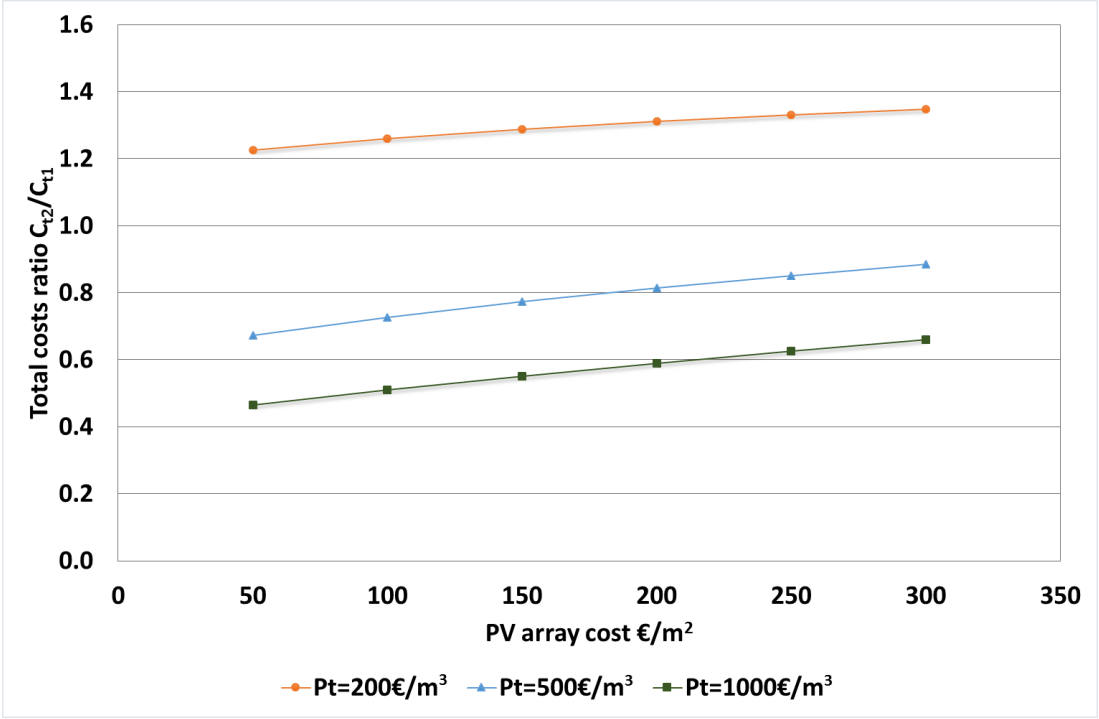

Fig. 17. Influence of the PV array cost in the total cost ratio for different tank costs and a battery cost of 250 €/kWh.

Fig. 18 shows the cost ratio C_{t2}/C_{t1} for a tank cost of 400 €/m^3 depending on the price of the PV array and different battery prices (P_b) for an evaporator temperature of 283 K.

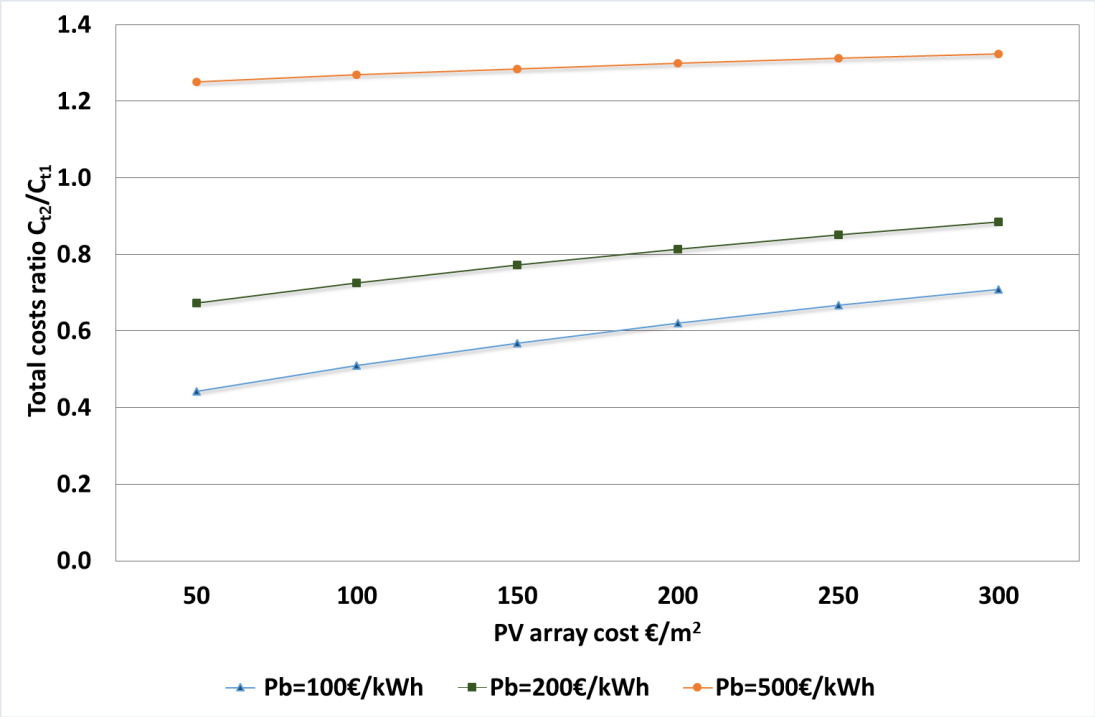

Fig. 18. Influence of the PV array cost in the total cost ratio for different battery cost and a tank cost of 400 €/kWh.

As shown Fig. 17 and 18, the cost ratio C_{t2}/C_{t1} increases when the cost of the PV array increases, but the influence of the PV array cost decreases as the battery and tank prices increase.

6. Conclusions

A novel storage system for stand-alone photovoltaic cooling installations has been described and analysed. This system is based on the use of a thermally insulated storage tank with ammonia in saturated mixture phase integrated into the vapour-compression cooling cycle. The tank volume and its maximum pressure have been determined, getting acceptable values.

The proposed installation is an economically viable alternative to the use of batteries for a wide range of evaporator and condenser temperatures and tank and battery costs. The installation would be economically viable in hot climates where the condenser temperature is high and for applications of food refrigeration and freezing where the evaporator temperature is low. The PV array cost does not have a significant influence on the results.

The practical feasibility of the proposed installation requires solving technological aspects of direct control between the heat pump and the PV array and internal control of the heat pump according to the operating modes proposed. This installation could pave the way for an alternative to energy storage in batteries for stand-alone photovoltaic cooling applications. It is likely suitable for remote villages where the grid is not available.

Author contribution statement

I. Lillo-Bravo: Conceptualization, Methodology, Investigation, Writing- Original draft preparation.

M. A. Bobadilla: Visualization, Investigation, Software.

S. Moreno-Tejera: Validation, Software, Writing- Reviewing and Editing.

M. Silva-Perez: Supervision. Declaration of competing interest

The authors declare that they have no known competing financial interests or personal relationships that could have appeared to influence the work reported in this paper.

Acknowledgments

This work was supported by the Andalusia Regional Government ('Junta de Andalucía') within the frame of the project CLIMACSOL (Project No. PI-1454/40/2015).

The authors wish to thank Professor Juan Francisco Coronel Toro (University of Seville) for his constructive remarks and useful guidelines.

REFERENCES

34-2007 (Standard ANSI/ASHRAE), 2007. Designation and Safety Classification of Refrigerants, in: American Cociety of Heating,Refrigerating and Air-Conditioning Engineers, Inc. Atlanta. p. ISSN 1041-2336.

Alobaid, M., Hughes, B., Calautit, J.K., O'Connor, D., Heyes, A., 2017. A review of solar driven absorption cooling with photovoltaic thermal systems. Renew. Sustain. Energy Rev. 76, 728–742. doi:10.1016/j.rser.2017.03.081

Alva, G., Liu, L., Huang, X., Fang, G., 2017. Thermal energy storage materials and systems for solar energy applications. Renew. Sustain. Energy Rev. 68, 693–706. doi:10.1016/j.rser.2016.10.021

Arenas, L.F., Ponce de León, C., Walsh, F.C., 2017. Engineering aspects of the design, construction and performance of modular redox flow batteries for energy storage. J. Energy Storage 11, 119–153. doi:10.1016/j.est.2017.02.007

Awadallah, M.A., Venkatesh, B., 2016. Accuracy improvement of SOC estimation in lithium-ion batteries. J. Energy Storage 6, 95–104. doi:10.1016/j.est.2016.03.003

Axaopoulos, P.J., Theodoridis, M.P., 2009. Design and experimental performance of a PV Ice-maker without battery. Sol. Energy 83, 1360–1369. doi:10.1016/j.solener.2009.03.007

Beccali, M., Finocchiaro, P., Nocke, B., 2009. Energy and economic assessment of desiccant

cooling systems coupled with single glazed air and hybrid PV/thermal solar collectors for applications in hot and humid climate. Sol. Energy 83, 1828–1846. doi:10.1016/j.solener.2009.06.015

Bilgili, M., 2011. Hourly simulation and performance of solar electric-vapor compression refrigeration system. Sol. Energy 85, 2720–2731. doi:10.1016/j.solener.2011.08.013

Bruch, M., Müller, M., 2014. Calculation of the cost-effectiveness of a PV battery system. Energy Procedia 46, 262–270. doi:10.1016/j.egypro.2014.01.181

Chen, H., Riffat, S.B., Fu, Y., 2011. Experimental study on a hybrid photovoltaic/heat pump system. Appl. Therm. Eng. 31, 4132–4138. doi:10.1016/j.applthermaleng.2011.08.027

Chua, K.J., Chou, S.K., Yang, W.M., 2010. Advances in heat pump systems: A review. Appl. Energy 87, 3611–3624. doi:10.1016/j.apenergy.2010.06.014

Fong, K.F., Chow, T.T., Lee, C.K., Lin, Z., Chan, L.S., 2010. Comparative study of different solar cooling systems for buildings in subtropical city. Sol. Energy 84, 227–244. doi:10.1016/j.solener.2009.11.002

Frigicoll Company, 2014. Suite 3D Solar. Kay-PV 3DN5 [WWW Document]. URL http://www.kaysun.es/es/productos/detalle/kay-pv-3dn5 (access on line on 24th November 2017)

Ge, T.S., Wang, R.Z., Xu, Z.Y., Pan, Q.W., Du, S., Chen, X.M., Ma, T., Wu, X.N., Sun, X.L., Chen, J.F., 2018. Solar heating and cooling: Present and future development. Renew. Energy 126, 1126–1140. doi:10.1016/j.renene.2017.06.081

Hu, H., Wang, R., Fang, G., 2010. Dynamic characteristics modeling of a hybrid photovoltaic-thermal heat pump system. Int. J. Green Energy 7, 537–551. doi:10.1080/15435075.2010.515446

Ji, J., Pei, G., Chow, T. tai, Liu, K., He, H., Lu, J., Han, C., 2008. Experimental study of photovoltaic solar assisted heat pump system. Sol. Energy 82, 43–52. doi:10.1016/j.solener.2007.04.006

Jossen, A., Garche, J., Sauer, D.U., 2004. Operation conditions of batteries in PV applications. Sol. Energy 76, 759–769. doi:10.1016/j.solener.2003.12.013

Keliang, L., Jie, J., Tin-tai, C., Gang, P., Hanfeng, H., Aiguo, J., Jichun, Y., 2009. Performance study of a photovoltaic solar assisted heat pump with variable-frequency compressor - A case study in Tibet. Renew. Energy 34, 2680–2687. doi:10.1016/j.renene.2009.04.031

Khan, M., Swierczynski, M., Kær, S., 2017. Towards an Ultimate Battery Thermal Management

System: A Review. Batteries 3, 9. doi:10.3390/batteries3010009

Klein, S.A., 1992. Engineering Equation Solver (EES) software.

Lazzarin, R.M., Noro, M., 2018. Past, present, future of solar cooling: Technical and economical considerations. Sol. Energy 172, 2–13. doi:10.1016/j.solener.2017.12.055

Lemmon, E.W., Mclinden, M.O., Huber, M.., 2002. REFPROP Reference Fluid Thermodynamic and Transport Properties. NIST Standard Reference Database 23.

Lillo-Bravo, I., Pérez-Aparicio, E., Sancho-Caparrini, N., Silva-Pérez, M.A., 2018. Benefits of Medium Temperature Solar Concentration Technologies as Thermal Energy Source of Industrial Processes in Spain. Energies 11. doi:10.3390/en11112950

Lillo, I., Silva, M., 2014. Thermodynamic limits of the use of solar energy for cold production, in: Proceeding of 28th European Photovoltaic Solar Energy Conference and Exhibition. Hamburg (Germany), pp. 3863–3868.

Lv, X., Song, J., Lai, Y., Fang, J., Li, J., Zhang, Z., 2016. Ultrafine nanoparticles assembled Mo2C nanoplates as promising anode materials for sodium ion batteries with excellent performance. J. Energy Storage 8, 205–211. doi:10.1016/j.est.2016.08.009

Ma, G.Y., Zhao, H.X., 2008. Experimental study of a heat pump system with flash-tank coupled with scroll compressor. Energy Build. 40, 697–701. doi:10.1016/j.enbuild.2007.05.003

Market realist [WWW Document], 2016. URL http://marketrealist.com/2016/09/ammonia-prices-continue-movement-last-week/ (access on line on 21st January 2017)

Mira-Hernández, C., Weibel, J.A., Groll, E.A., Garimella, S. V., 2016. Compressed-liquid energy storage with an adsorption-based vapor accumulator for solar-driven vapor compression systems in residential cooling. Int. J. Refrig. 64, 176–186. doi:10.1016/j.ijrefrig.2015.11.015

Onur, E., Ugur Sava, S., 2011. The Effect of inverter efficiency on stand-alone residential PV system sizing, in: 7th International Conference on Electrical and Electronics Engineering (ELECO). pp. 317–319.

Oró, E., de Gracia, A., Castell, A., Farid, M.M., Cabeza, L.F., 2012. Review on phase change materials (PCMs) for cold thermal energy storage applications. Appl. Energy 99, 513–533. doi:10.1016/j.apenergy.2012.03.058

Otanicar, T., Taylor, R.A., Phelan, P.E., 2012. Prospects for solar cooling - An economic and environmental assessment. Sol. Energy 86, 1287–1299. doi:10.1016/j.solener.2012.01.020

Ozcan, H., Akyavuz, U.D., 2017. Thermodynamic and economic assessment of off-grid portable cooling systems with energy storage for emergency areas. Appl. Therm. Eng. 119, 108–118. doi:10.1016/j.applthermaleng.2017.03.046

Palomba, V., Wittstadt, U., Bonanno, A., Tanne, M., Harborth, N., Vasta, S., 2019. Components and design guidelines for solar cooling systems: The experience of ZEOSOL. Renew. Energy 141, 678–692. doi:10.1016/j.renene.2019.04.018

Pintaldi, S., Perfumo, C., Sethuvenkatraman, S., White, S., Rosengarten, G., 2015. A review of thermal energy storage technologies and control approaches for solar cooling. Renew. Sustain. Energy Rev. 41, 975–995. doi:10.1016/j.rser.2014.08.062

PV-magazine [WWW Document], 2016. URL https://www.pv-magazine.com/features/investors/module-price-index/ (access on line on 22nd september 2017)

Rajani, S.V., Pandya, V.J., 2016. Experimental verification of the rate of charge improvement using photovoltaic MPPT hardware for the battery and ultracapacitor storage devices. Sol. Energy 139, 142–148. doi:10.1016/j.solener.2016.09.037

Saitoh, H., Hamada, Y., Kubota, H., Nakamura, M., Ochifuji, K., Yokoyama, S., Nagano, K., 2003. Field experiments and analyses on a hybrid solar collector. Appl. Therm. Eng. 23, 2089–2105. doi:10.1016/S1359-4311(03)00166-2

Sampaio, P.G.V., González, M.O.A., 2017. Photovoltaic solar energy: Conceptual framework. Renew. Sustain. Energy Rev. 74, 590–601. doi:10.1016/j.rser.2017.02.081

Sarbu, I., Sebarchievici, C., 2013. Review of solar refrigeration and cooling systems. Energy Build. 67, 286–297. doi:10.1016/j.enbuild.2013.08.022

Shuru, C., Jianming, Z., Lu, Y., Xiaodi, R., Mark, H.E., Chaojiang, N., Hongkyung, L., Xu, W., Xiao, J., Liu, J., Zhang, J.-G., 2018. High-Efficiency Lithium Metal Batteries with Fire-Retardant Electrolytes. Joule 2, 1548–1558.

Solaray energy [WWW Document], 2013. URL http://solaray.com.au/how-much-do-solar-batteries-cost/ (access on line on 22nd september 2017)

Torres-Toledo, V., Meissner, K., Täschner, P., Martınez-Ballester, S., Müller, J., 2016. Design and performance of a small-scale solar ice-maker based on a DC-freezer and an adaptive control unit. Sol. Energy 139, 433–443. doi:10.1016/j.solener.2016.10.022

Veerakumar, C., Sreekumar, A., 2016. Phase change material based cold thermal energy storage: Materials, techniques and applications - A review. Int. J. Refrig. 67, 271–289.

doi:10.1016/j.ijrefrig.2015.12.005

Visek, M., Joppolo, C.M., Molinaroli, L., Olivani, A., 2014. Advanced sequential dual evaporator domestic refrigerator/freezer: System energy optimization. Int. J. Refrig. 43, 71–79. doi:10.1016/j.ijrefrig.2014.03.001

Wang, F., Maidment, G., Missenden, J., Tozer, R., 2007a. The novel use of phase change materials in refrigeration plant. Part 1: Experimental investigation. Appl. Therm. Eng. 27, 2893–2901. doi:10.1016/j.applthermaleng.2005.06.011

Wang, F., Maidment, G., Missenden, J., Tozer, R., 2007b. The novel use of phase change materials in refrigeration plant. Part 2: Dynamic simulation model for the combined system. Appl. Therm. Eng. 27, 2902–2910. doi:10.1016/j.applthermaleng.2005.06.009

Wang, F., Maidment, G., Missenden, J., Tozer, R., 2007c. The novel use of phase change materials in refrigeration plant. Part 3: PCM for control and energy savings. Appl. Therm. Eng. 27, 2911–2918. doi:10.1016/j.applthermaleng.2005.06.010

Wang, X., Hwang, Y., Radermacher, R., 2009. Two-stage heat pump system with vapor-injected scroll compressor using R410A as a refrigerant. Int. J. Refrig. 32, 1442–1451. doi:10.1016/j.ijrefrig.2009.03.004

Xie, Y., Song, L., Liu, C., 2006. Analysis of a solar assisted heat pump dryer with a storage tank, in: 2006 ASME International of Solar Energy Conference. Denver.

Xu, Q., Ji, Y.N., Qin, L.Y., Leung, P.K., Qiao, F., Li, Y.S., Su, H.N., 2018. Evaluation of redox flow batteries goes beyond round-trip efficiency: A technical review. J. Energy Storage 16, 108–115. doi:10.1016/j.est.2018.01.005

Xu, S.M., Huang, X.D., Du, R., 2011. An investigation of the solar powered absorption refrigeration system with advanced energy storage technology. Sol. Energy 85, 1794–1804. doi:10.1016/j.solener.2011.04.022